Downlink MAC Scheduler for 5G Communications with Spatial Focusing Effects

Zhung-Han Wu, *Student Member, IEEE,* Beibei Wang, *Senior Member, IEEE,* Chunxiao Jiang, *Senior Member, IEEE,* and K. J. Ray Liu, *Fellow, IEEE*

***Abstract*—Driven by the demand for supporting the rapidly increasing wireless traffic, the next generation communication system, i.e. the 5G system, needs to accommodate a massive number of users and judiciously manage the interference. One promising candidate, the time reversal (TR) system, uses a large bandwidth and designs transmitting waveforms such that the environment acts as a matched filter and the transmitted signal adds up coherently at the intended users. Therefore the energy is focused only at the intended users with reduced interference to others. The other candidate, massive MIMO system utilize a large number of antennas to focus the energy to the users and reduce the mutual interference. However, the massive number of users poses a limit on system performance due to increasing interuser interference (IUI) and the system has to make a judicial selection of transmitting users. In this work, we propose a scheduler that maximizes the system weighted sum rate while satisfying the minimum rate requirements of the transmitting users. The optimization problem is transformed into a mixed integer quadratically constrained quadratic programming (MIQCQP) with linear time complexity. We also investigate the impact of imperfect channel information on the proposed scheduler algorithm and reveal similar channel estimation error distribution between the TR and massive MIMO system. We evaluate the performance of the proposed scheduler in different scenarios and the results show that the proposed scheduler has several desirable characteristics, including low time complexity, suitable on versatile system structure, and robustness against imperfect channel information.**

***Index Terms*—**Time reversal, spatial focusing, massive MIMO, scheduler.

I. Introduction

RECENT achievements of manufacturing technology and the reduced cost of wireless communication devices have led to a revolutionary concept of Internet of Things (IoT). The interconnected everyday appliances monitor useful information that facilitates everyday chores, responds to environment changes in time, and discovers activity patterns from the massive collected data. The IoT vision relies heavily on the ability that the communication system accommodates and coordinates the massive number of users in the system simultaneously. Therefore, the ability of the next generation communication system, i.e. the 5G system, to support a massive number of users while maintaining service quality is high desirable.

The time reversal (TR) system is proposed as a candidate system for IoT [1] as well as for 5G communication [2] that possesses several strengths, such as supporting a large number of low-cost terminal devices, versatility and heterogeneity in bandwidth use, and easy scalability in network densification. The TR system utilizes a large bandwidth and observes a lot of channel impulse response (CIR) taps compared to the narrowband communication system in which only two to three channel taps can be observed. The CIR is composed of the superposition of the randomly reflected transmitted signals from multipath-rich environments such as in the indoor environment with structures and objects. Because the CIRs naturally embed the information about the environment, experiments show that the CIRs are location-specific and the CIRs can be used for precise indoor localization [3].

The location-specific CIR benefits the TR system with the spatial focusing effect [3] that focuses the transmitted energy to the intended user. By selecting the waveform signature as the time-reversed and conjugated version of the intended receiver's CIR, the transmitted waveform adds up constructively at the exact location of the intended receiver, while the waveform adds up randomly at all other locations. The receiver receives maximum signal energy with small energy leakage to surrounding users. The energy focusing due to location-specific CIR information separates TR users operating on the same frequency band and allows simultaneous access, leading to the design of time reversal division multiple access (TRDMA) system that provides service to a large amount of users [4].

The other 5G candidate, the massive MIMO system, achieves the energy focusing by using a large number of antennas [5]. The massive MIMO system concentrates the transmitted energy at the intended user by adjusting the weight vector of the antennas, which is known as beamforming. With the increase of the number of antennas, the massive MIMO system directs the energy to more intended users with small energy leakage to the unintended users, and therefore the system is able to support lots of users.

With the ever-increasing number of users in the foreseeable IoT future, the 5G systems cannot indefinitely support all users simultaneously due to the fixed usable bandwidth and/or the fixed number of antennas. Interference among the users will increase and the energy focusing effect can no longer support the massive users with a satisfactory quality of service (QoS). As a result, a system scheduler that dictates when and whom to access the system simultaneously and maximizes the system performance is desirable. The scheduler also requires a reasonable complexity in order to operate in real time with strict scheduling deadlines.

The authors are with Origin Wireless, Inc., Greenbelt, MD 20770, USA. Z. Wu, B. Wang and K. J. R. Liu are with the Department of Electrical and Computer Engineering, University of Maryland, College Park, MD 20742, USA. C. Jiang is with the Tsinghua Space Center, Tsinghua University, Beijing 100084, China.(email: {zhwu, bebewang, kjrliu}@umd.edu, jchx@tsinghua.edu.cn)

Manuscript received May 6, 2016; revised September 15, 2016.

Many existing systems already have schedulers deployed, however, none can be implemented directly on the TR and the massive MIMO system. There are two main reasons. The first is the fundamental differences in the physical layer design. In existing and widely deployed OFDMA systems, such as the LTE system, the scheduler allocates the resource blocks (RBs) that are mutually orthogonal in time and frequency to users. The RBs are allocated based on system requirements such as the QoS awareness of the users [6]–[8] or the weighted sum rate of the overall system [9]. However, in the case of TR system, the transmission resource is not mutually orthogonal and all the users are using the same transmission band. Therefore a new scheduler design is needed to select a subset of users for transmission while managing the in-band interference. On the other hand, although OFDMA can be an element for massive MIMO system, the interference between users still exists for the users on the same frequency band and interference management is still desirable.

The second reason is that with the massive number of users in the system, it is possible that the system cannot accommodate the users simultaneously via power control. In a typical power control scheme, the system adjusts the transmit power to different users in order to control the interference introduced to unintended users [10]–[12]. However, when a massive number of users are present in the system, all the proposed power allocation based algorithm might not be feasible due to minimum transmitted power requirements of the users. The system therefore needs to efficiently select a subset of users for transmission that not only maximizes the system objective but also meets the individual QoS requirements.

In a scheduler design, it is usually assumed perfect channel information, whereas the channel information is imperfect in reality. Several factors contribute to the imperfect channel information including the aging of the channel, the received noise during channel estimation, the pilot contamination between users, and so on. The imperfect channel information not only degrades the performance of the physical layer but also deteriorates the scheduler performance. Robustness against imperfect channel information in scheduler design is therefore highly desirable to sustain the system performance when the channel information is inaccurate.

In order to address the above issues, we propose a novel medium access control (MAC) layer scheduler design by taking into consideration of the unique focusing effect for both the TR and massive MIMO system. In the first part of the paper, we focus on the scheduler algorithm that selects a subset of users and maximizes the system weighted sum rate. The optimization problem is transformed and formulated as a mixed integer quadratically constrained quadratic program (MIQCQP) [13] where the optimization problem is solved using an optimization solver. In the second part, we focus on the impact of imperfect channel information on the scheduler performance. We analyze a channel estimation scheme for TR system proposed in [14] and identify similar channel estimation error distribution as in the massive MIMO case. We evaluate the robustness of the proposed scheduler against imperfect channel information provided by the channel estimation scheme.

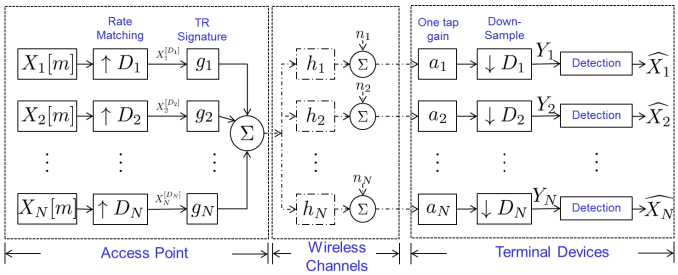

Fig. 1: System diagram of a TRDMA system.

The main contribution of this paper can be summarized as follows:

1) We propose an efficient scheduler algorithm for the 5G system that maximizes the weighted sum rate by selecting a subset of users for transmission. The system objective and QoS constraints are transformed into an MIQCQP with empirical linear time complexity.
2) We analyze the channel estimation error distribution of the TR system. The analysis shows that the TR channel estimation scheme reduces the channel estimation error power and reveals a similar estimation error distribution as in the massive MIMO case.
3) We evaluate the proposed scheduler under imperfect channel information. Experiment results show that the proposed scheduler is robust against imperfect channel information with small performance degradation.

The paper is organized as follows. System description for both the TR and massive MIMO system is given in Sec.II. The energy focusing effect of both TR and massive MIMO systems is illustrated via simulation in Sec.III. The scheduler objective and user requirements are described in Sec.IV and the MIQCQP formulation is developed. In Sec.V, we investigate the impact of the imperfect channel information on the performance of the scheduler. Simulation results are presented in Sec.VI where the performance of the scheduler is evaluated under various settings. Finally, a conclusion is given in Sec.VII.

II. System Overview

We give brief overviews of the TRDMA downlink system and the massive MIMO downlink system and introduce the spatial focusing effect of both systems.

A. Time Reversal Division Multiple Access System

A schematic view of a TRDMA downlink system is depicted in Fig.1, where N users/terminal devices (TD) are served. The access point (AP) first upsamples the symbol stream for user i by the backoff factor D_i. The upsampled symbols are encoded using the corresponding waveforms $\mathbf{g}_i$ which are assigned to the users. The AP transmits the summed signal with a single antenna and the transmitted signal passes through individual users' channels $\mathbf{h}_i$. The users adjust the power using one tap gain, downsample the received signal and then perform detection to estimate and recover the transmitted symbols.

This article has been accepted for publication in a future issue of this journal, but has not been fully edited. Content may change prior to final publication. Citation information: DOI 10.1109/TWC.2017.2690432, IEEE Transactions on Wireless Communications

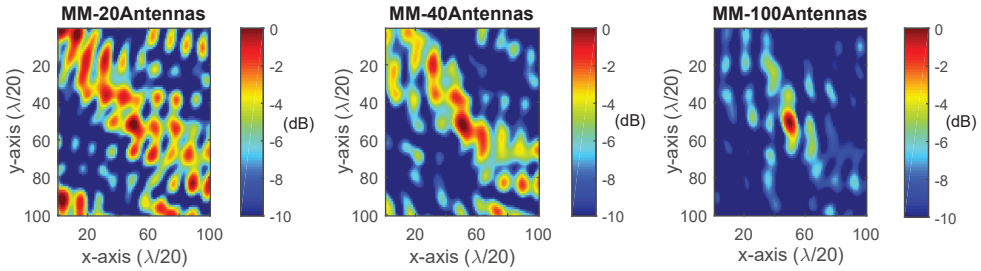

(a) Normalized field strength in a $5\lambda \times 5\lambda$ area centered around the receiver of a massive MIMO system.

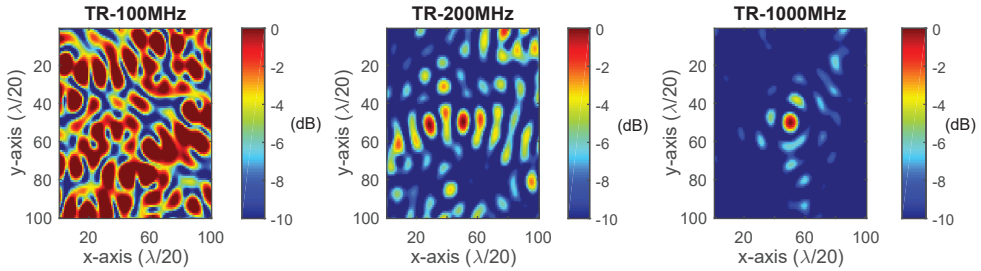

(b) Normalized field strength in a $5\lambda \times 5\lambda$ area centered around the receiver of a TR system.

Fig. 2: Demonstration of the spatial focusing effect for both TR and massive MIMO systems with different DoF.

Using the time reversed and conjugated CIR $\mathbf{h}_i$ between the AP and user i as the waveform $\mathbf{g}_i$, user i obtains the maximum signal power. However, the interuser interference (IUI) and intersymbol interference (ISI) reduce the SINR of users and therefore the TR waveform $\mathbf{g}_i$ can be specifically and jointly designed for the system to meet system requirements. Several waveform design algorithms have been proposed in [15] and [16] to alleviate IUI and ISI and to increase the SINR.

B. Massive MIMO system

Suppose that there are M antennas in the base station serving K one-antenna terminal devices. The channel $\mathbf{h}_i^M$ from the base station to the user i is an M by 1 vector where the jth element is the channel from the jth antenna to the ith user. We assume a narrowband massive MIMO system which observes one tap channel due to the limited subcarrier granularity. Proper beamforming vectors $\mathbf{g}_i^M$ can be designed to steer the energy to the intended user i, such as the maximum-ratio transmission and zero-forcing beamforming in [17].

The TR system utilizes the time-reversed and conjugated CIR as precoding waveform to transmit the energy to the specific users. Because the CIR are location-specific [3], the energy only concentrates at the intended users with small energy leakage to the surroundings, which is called the spatial focusing effect. The large bandwidth enables the TR system to resolve more taps from location-specific channels and focuses the energy more sharply to the intended user. On the other hand, the massive MIMO system focuses the energy to the intended users using the maximum-ratio-combining beamforming weights. By installing more and more antennas, the massive MIMO system concentrates the energy more sharply at the intended users as the TR system does with a larger bandwidth. The spatial focusing effect resulting from either larger bandwidth or more antennas enables the 5G system to pinpoint the energy to the exact users, to reduce the interference leakage, and therefore to accommodate more users than that in existing systems. In order to illustrate the spatial focusing phenomenon, we conduct a simulation in both TR and massive MIMO systems to reveal how the focusing effect becomes prominent with the increase in either bandwidth or the number of antennas.

III. Spatial Focusing Effect

With proper waveform design $\mathbf{g}_i$ and beamform weight design $\mathbf{g}_i^M$, both the systems focus energy only at the intended users. The ability of the energy transmission targeting at specific users is affected by the degree of freedom (DoF) of the design, which is the number of variables in $\mathbf{g}_i$ or $\mathbf{g}_i^M$. The TR system increases the DoF by using a large bandwidth which results in a massive number of observed CIR taps, while the massive MIMO system increases the DoF by installing a massive number of antennas. The larger the bandwidth and the number of antennas, the larger DoF, and therefore the better spatial energy focusing at the locations of the intended users.

To illustrate the spatial focusing effect of both systems with different DoF, we conduct a simulation based on ray-tracing techniques in a discrete scattering environment. 400 scatterers are distributed randomly in a $200\lambda \times 200\lambda$ area, where λ is the wavelength corresponding to the carrier frequency of the system. The wireless channel is simulated by calculating the sum of the multipaths using the ray-tracing method given the locations of the scatterers. Without loss of generality, we use a single-bounce ray-tracing method to calculate the channels for both the TR system and the massive MIMO system on the 5GHz ISM band. We select the reflection coefficients of the scatterers to be i.i.d. complex random variables with uniform distribution in amplitude $[0, 1]$ and phase $[0, 2\pi]$. For

the massive MIMO system, the linear array is configured with the line facing the scattering area and the interval between two adjacent antennas is $\lambda/2$. The distance from the transmitter and the intended location is chosen to be 500λ for both systems.

To show the effect of system DoF on the spatial focusing effect, we adjust the transmitting bandwidth of the TR system and the number of antennas in the massive MIMO system. The transmitter of the TR system transmits with bandwidths ranging from 100 MHz to 1GHz with one antenna, where a wider bandwidth observes more CIR taps and increases the system DoF. The number of antennas in the massive MIMO system is selected from 20 to 100 with bandwidth fixed at 1MHz in the simulation. We select the matched filter waveform and beamforming weights in the TR system and the massive MIMO system, respectively.

We consider the received energy strength in a $5\lambda \times 5\lambda$ area around the location of the intended user. Fig. 2 shows the simulation results for both systems with a single channel and scatterer realization, and we normalize the maximum received energy to 0dB. We can see that the energy focusing effect becomes more obvious at the intended location with the increase in the bandwidth and the number of antenna, which is the result of larger DoF to concentrate the energy at only the intended users.

However, a closer look at the energy field in Fig. 2 reveals that even with large transmitting bandwidth and a massive number of antennas, energy leakage still occurs at the surrounding of the intended users. The energy leakage causes the IUI and the interference level increases when the number of users grows. Scheduler design is therefore desirable to perform interference management by selecting a subset of users for transmission. In essence, the user selection is to choose a subset of users such that the energy leakage has small interference to any of the other selected users in order to reduce the IUI and to increase the total transmission rate.

IV. Downlink User Selection Algorithm

In this section, we detail the algorithm for maximizing the weighted sum rate in the downlink system. To be specific, the scheduler receives the normalized interference matrix and the allocated transmission power for each of the users from the physical layer and the minimum required transmission rate for the user from the application layer. The scheduler maintains weights for the users to adjust the fairness and to avoid starving due to poor channel condition and shadowing. Based on the information, the scheduler selects a subset of users to transmit simultaneously and maximizes the weighted sum rate while satisfying the minimum SINR requirement for the selected users.

A. TRDMA System Overview

First let us characterize the received signal of the users in a TRDMA downlink system. Suppose that there are N users in the system and all users use the same backoff factor D. $X_i[m]$ is the transmitted symbols to user i, which is assumed to be i.i.d. with unit power. Based on the system structure in Fig. 1, the transmit signal of the AP can be expressed as

$$s[m] = \sum_i \sum_l \sqrt{p_i}\mathbf{g}_i[m-l]X_i^{[D]}[l], \tag{1}$$

where $X_i^{[D]}$ represents the upsampled version of the symbols to user i by D, p_i is the allocated transmit power and $\mathbf{g}_i$ denotes the designed transmitting waveform with unit power for user i. User i receives the signal and downsamples the signal for detection, and the downsampled signal can be expressed as

$$\begin{aligned} Y_i[m] &= \sum_{j=1}^{N}\sum_l \sqrt{G_j p_j}X_j[l](\mathbf{h}_i * \mathbf{g}_j)[mD-lD] + n_i[m] \\ &= \sqrt{G_i p_i}X_i[m](\mathbf{h}_i * \mathbf{g}_i)[L-1] \\ &\quad + \sqrt{G_i p_i}\sum_{l=0,l\neq\frac{L-1}{D}}^{\frac{2L-2}{D}} X_i[m-l](\mathbf{h}_i * \mathbf{g}_i)[Dl] \\ &\quad + \sum_{j\neq i}\sqrt{G_i p_j}\sum_{l=0}^{\frac{2L-2}{D}} X_j[m-l](\mathbf{h}_i * \mathbf{g}_j)[Dl] + n_i[m], \end{aligned} \tag{2}$$

where $\mathbf{h}_i$ is the channel from AP to user i with unit power. L is the length of $\mathbf{h}_i$, which depends on the delay spread of the environment and the utilized bandwidth of the system. With our measurement using TR system prototype with 125 MHz bandwidth, we observe about 10 significant CIR taps and the total channel length L is about 30. For notation brevity, we assume that $L-1$ is an integer multiple of the backoff factor D. G_i is the path gain from the AP to user i. Note that the $\mathbf{h}_i$ is unit power and the channel power is absorbed into G_i. n_i is the receiving noise of user i and is assumed to be an i.i.d. complex Gaussian r.v. with power σ_i^2. In (2), the first term represents the intended signal for user i; the second term is the ISI; the third term is the IUI and the last term is the receiving noise.

B. Normalized Interference Matrix Calculation

Let us characterize the interference between the users based on the unit power channel $\mathbf{h}_i$ and the waveforms $\mathbf{g}_i$. The $(i,j)^{th}$ entry $\mathbf{Z}_{i,j}$ of the normalized interference matrix $\mathbf{Z}$ refers to the interference from user j to user i. Therefore, $\mathbf{Z}_{i,j}$ is determined by the channel $\mathbf{h}_i$ from the AP to the user i and the waveform $\mathbf{g}_j$ used to transmit to user j. $\mathbf{Z}_{i,j}$ is calculated using unit power $\mathbf{h}_i$ and unit power $\mathbf{g}_j$, and therefore the name normalized interference matrix. We separate p_j in the calculation of $\mathbf{Z}_{i,j}$ because the power allocation and the waveforms are not necessarily designed together and the separation expands the occasions where the scheme is applicable. Based on (2), the normalized interference between users can therefore be represented as

$$\mathbf{Z}_{i,j} = \sum_{l=0}^{\frac{2L-2}{D}} \left|(\mathbf{h}_i * \mathbf{g}_j)[Dl]\right|^2, \tag{3}$$

$$\mathbf{Z}_{i,i} = \sum_{\substack{l=0 \\ l \neq \frac{L-1}{D}}}^{\frac{2L-2}{D}} |(\mathbf{h}_i * \mathbf{g}_i)[Dl]|^2, \tag{4}$$

where (3) and (4) are the IUI and ISI for user i, respectively. On the other hand, the IUI for the massive MIMO system can be calculated as

$$\mathbf{Z}_{i,j} = \left|(\mathbf{h}_i^M)^T \mathbf{g}_j^M\right|^2, \tag{5}$$

there is no ISI in the massive MIMO system due to the assumption of limited subcarrier granularity and a single tap channel is observed.

C. Scheduler Objective

Let us first formulate the scheduler objective and the constraints. Suppose that the physical layer provides the scheduler with the normalized interference matrix $\mathbf{Z}$ between users, the allocated power $\mathbf{p}$ and the path gain G_i between the AP and user i. The scheduler gathers the transmission rate requirements R_i from the application layer for proper operation if user i is selected to transmit. For a specific transmission rate requirements R_i, we can obtain the corresponding minimum SINR requirement γ_i by the one to one mapping between rate and SINR. The scheduler maintains a set of weights w_i to indicate the relative importance of each user. Based on the collected information and requirement, the scheduler objective that maximizes the system weighted sum rate is formulated as

$$\begin{aligned} &\underset{\mathbf{x}}{\text{maximize}} \ \sum_i w_i x_i \log_2\left(\frac{G_i p_i}{G_i \sum_j p_j \mathbf{Z}_{i,j} x_j + \sigma_i^2} + 1\right) \\ &\text{subject to } x_i \in \{0,1\}, \quad \sum_i p_i x_i \leq P_{max}, \\ &\qquad \frac{G_i p_i x_i}{G_i \sum_j p_j \mathbf{Z}_{i,j} x_j + \sigma_i^2} \geq \gamma_i x_i, \forall i. \end{aligned} \tag{6}$$

The first constraint requires the decision variables x_i to be binary, and $x_i = 1$ represents user i is selected to transmit. The second constraint requires that the sum of the transmitting power of the selected users to be no more than the maximum AP transmitting power. The third set of constraints corresponds to the minimum SINR requirements γ_i that the selected users must meet, and therefore the selected users meet the minimum transmission rate requirement R_i.

D. Mixed Integer Optimization

Let us describe the optimization transformation here. By enumerating all possible $\mathbf{x}$ vectors, we can find the optimal decision vector $\mathbf{x}_{opt}$ that maximized the objective and meet all the SINR constraints. However, the complexity for complete enumeration grows exponentially with the number of users N and therefore enumeration is not feasible when the number of users grows big. In this section, we propose a simple yet effective problem formulation that transforms the objective and the constraints into an MIQCQP problem.

One property for binary decision variables that is used in the optimization formulation is as follows,

$$x_i^2 = x_i, \quad \forall i. \tag{7}$$

This relationship helps convert some of the quadratic terms into linear terms in the system objective and the constraints.

We consider that the scheduler operates in the high SNR region where we omit the noise term σ_i^2 at the receiver and the plus 1 term in the logarithm function. Also, the path gain G_i cancels each other and the optimization objective becomes

$$\begin{aligned} &\underset{\mathbf{x}}{\text{maximize}} \ \sum_i w_i x_i \log_2\left(\frac{p_i}{\sum_j p_j \mathbf{Z}_{i,j} x_j}\right) \\ &\text{subject to } x_i \in \{0,1\}, \quad \sum_i p_i x_i \leq P_{max} \\ &\qquad \frac{p_i x_i}{\sum_j p_j \mathbf{Z}_{i,j} x_j + \sigma_i^2 / G_i} \geq \gamma_i x_i, \forall i \end{aligned} \tag{8}$$

We decompose the objective function into two terms using characteristics of the logarithm function as the following

$$\begin{aligned} &\underset{\mathbf{x}}{\text{maximize}} \ \sum_i w_i x_i \log_2\left(\frac{p_i}{\sum_j p_j \mathbf{Z}_{i,j} x_j}\right) \\ \equiv \ &\underset{\mathbf{x}}{\text{maximize}} \ \sum_i w_i x_i \ln p_i - \sum_i x_i w_i \ln\left(\sum_j p_j \mathbf{Z}_{i,j} x_j\right). \end{aligned} \tag{9}$$

Next, we linearize the second logarithm term using the Taylor expansion of logarithm at $x_0 = 1$ and use the constant term and the first order term. Note that the Taylor expansion for logarithm function to the linear term is a global overestimator of the logarithm function.

Let $\mathbf{p}$, $\mathbf{w}$ be the power and weight vector of length N of the users respectively. The second term in (9) can be simplified as

$$\begin{aligned} &\sum_i w_i x_i \ln\left(\sum_j p_j \mathbf{Z}_{i,j} x_j\right) \\ &\leq \ \sum_i w_i x_i \left(\sum_j p_j \mathbf{Z}_{i,j} x_j\right) - \mathbf{w}^T \mathbf{x} \\ &= \ \mathbf{x}^T \left(\text{diag}(\mathbf{w}) \mathbf{Z} \text{diag}(\mathbf{p})\right) \mathbf{x} - \mathbf{w}^T \mathbf{x}, \end{aligned} \tag{10}$$

where diag$(\cdot)$ operation generates a diagonal matrix using the elements in the vector. The inequality comes from the upper bound of Taylor expansion of the natural logarithm to the linear term. Define $\mathbf{A} = \text{diag}(\mathbf{w})\mathbf{Z}\text{diag}(\mathbf{p})$ and $\circ$ as the Hadamard product of two vectors. The objective function can be represented as

$$\sum_i w_i x_i \ln\left(\frac{p_i}{\sum_j p_j \mathbf{Z}_{i,j} x_j}\right) \tag{11a}$$

$$\geq \ (\ln(\mathbf{p}) \circ \mathbf{w})^T \mathbf{x} - \mathbf{x}^T \mathbf{A} \mathbf{x} + \mathbf{w}^T \mathbf{x} \tag{11b}$$

$$= \ (\ln(\mathbf{p}) \circ \mathbf{w} + \mathbf{w})^T \mathbf{x} - \frac{1}{2} \mathbf{x}^T (\mathbf{A} + \mathbf{A}^T) \mathbf{x}, \tag{11c}$$

where (11b) follows the property of Taylor expansion. The original objective function is transformed into (11c). However, it is not guaranteed that the optimal vector $\mathbf{x}_{opt}$ for (9) and (11c) are the same.

Define $\mathbf{I}_N$ as an identity matrix of size N and $\mathbf{1}$ be an all 1 vector of corresponding size, we add $\frac{c}{2}\mathbf{x}^T \mathbf{I}_N \mathbf{x}$ and subtract $\frac{c}{2}\mathbf{1}^T \mathbf{x}$ which have the same value by the property in (7), where c is a constant larger than the smallest eigenvalue of $\mathbf{A} + \mathbf{A}^T$.

Since the same value is added and subtracted in the objective, it does not change the objective value nor the feasible set. The reason for this redundancy will be discussed in Sec.IV-E. Define $\mathbf{Q} = \mathbf{A} + \mathbf{A^T} + c\mathbf{I}_N$, we arrive at the final formulation as

$$\begin{aligned} &\underset{\mathbf{x}}{\text{maximize}}\ (\ln(\mathbf{p}) \circ \mathbf{w} + \mathbf{w})^T\mathbf{x} - \frac{1}{2}\mathbf{x}^T(\mathbf{A} + \mathbf{A}^T)\mathbf{x} \\ \equiv\ &\underset{\mathbf{x}}{\text{minimize}}\ \frac{1}{2}\mathbf{x}^T(\mathbf{A} + \mathbf{A}^T + c\mathbf{I}_N)\mathbf{x} \\ &\qquad - (\ln(\mathbf{p}) \circ \mathbf{w} + \mathbf{w} + \frac{c}{2}\mathbf{1})^T\mathbf{x} \\ \equiv\ &\underset{\mathbf{x}}{\text{minimize}}\ \frac{1}{2}\mathbf{x}^T\mathbf{Q}\mathbf{x} - (\ln(\mathbf{p}) \circ \mathbf{w} + \mathbf{w} + \frac{c}{2}\mathbf{1})^T\mathbf{x}. \end{aligned} \tag{12}$$

The second constraint can be written as

$$\mathbf{p}^T\mathbf{x} \le P_{max} \tag{13}$$

For the third constraint, we have the minimum SINR constraint for user i as,

$$\frac{p_i x_i}{\sum_j p_j \mathbf{Z}_{i,j} x_j + \sigma_i^2/G_i} \ge \gamma_i x_i \tag{14a}$$

$$\equiv\ x_i \sum_j p_j \mathbf{Z}_{i,j} x_j + (\frac{\sigma_i^2}{G_i} - \frac{p_i}{\gamma_i})x_i \le 0, \tag{14b}$$

Let $\mathbf{0}_{n,m}$ be a n by m all zero matrix. Define B_i as an all zero matrix with ith row to be the Hadamard product of $\mathbf{z}_i$, the ith row of $\mathbf{Z}$, and the transpose of the power allocation vector $\mathbf{p}$ as follows

$$B_i = \begin{bmatrix} \mathbf{0}_{i-1,N} \\ \mathbf{z}_i \circ \mathbf{p}^T \\ \mathbf{0}_{N-i,N} \end{bmatrix}. \tag{15}$$

Define $\mathbf{q}_i$ as an all zero vector of length N, except for the ith component being $\sigma^2/G_i - p_i/\gamma_i$,

$$\mathbf{q}_i = \begin{bmatrix} \mathbf{0}_{i-1,1} \\ \frac{\sigma^2}{G_i} - \frac{p_i}{\gamma_i} \\ \mathbf{0}_{N-i,1} \end{bmatrix}. \tag{16}$$

Then the constraint can be represented as

$$\begin{aligned} &\mathbf{x}^T\mathbf{B}_i\mathbf{x} + \mathbf{q}_i^T\mathbf{x} \le 0,\ \forall i \\ \equiv\ &\frac{1}{2}\mathbf{x}^T(\mathbf{B}_i + \mathbf{B}_i^T + c_i\mathbf{I}_N)\mathbf{x} + (\mathbf{q}_i^T - \frac{c_i}{2}\mathbf{1})\mathbf{x} \le 0,\ \forall i, \\ \equiv\ &\frac{1}{2}\mathbf{x}^T\mathbf{Q}_i\mathbf{x} + (\mathbf{q}_i^T - \frac{c_i}{2}\mathbf{1})\mathbf{x} \le 0,\ \forall i \end{aligned} \tag{17}$$

where $\mathbf{Q}_i = \mathbf{B}_i + \mathbf{B}_i^T + c_i\mathbf{I}_N$. c_i is a constant that is larger than the minimum eigenvalue of $\mathbf{B}_i + \mathbf{B}_i^T$.

Based on the above transformation, the whole optimization problem is formulated as

$$\begin{aligned} &\underset{\mathbf{x}}{\text{minimize}}\ \frac{1}{2}\mathbf{x}^T\mathbf{Q}\mathbf{x} - (\ln(\mathbf{p}) \circ \mathbf{w} + \mathbf{w} + \frac{c}{2}\mathbf{1})^T\mathbf{x} \\ &\text{subject to}\ x_i \in \{0,1\}, \quad \mathbf{p}^T\mathbf{x} \le P_{max} \\ &\qquad \frac{1}{2}\mathbf{x}^T\mathbf{Q}_i\mathbf{x} + (\mathbf{q}_i^T - \frac{c_i}{2}\mathbf{1})\mathbf{x} \le \mathbf{0}, \forall i, \end{aligned} \tag{18}$$

which is an MIQCQP problem if and only if $\mathbf{Q}$ and $\mathbf{Q}_i$s are positive semidefinite.

E. Positive Semidefiniteness of $\mathbf{Q}$ *and* $\mathbf{Q}_i$

To ensure the transformed optimization problem to be an MIQCQP problem, we need to ensure $\mathbf{Q}$ and $\mathbf{Q}_i$ are all positive semidefinite. We first introduce the Weyl theorem [18] which states as follows.

Theorem 1: Let $\mathbf{U}$, $\mathbf{V}$ be Hermitian matrices of size N and let the eigenvalues $\lambda_i(\mathbf{U})$, $\lambda_i(\mathbf{V})$, and $\lambda_i(\mathbf{U}+\mathbf{V})$ be arranged in non-decreasing order. For $k = 1, 2, \cdots, N$, we have

$$\lambda_k(\mathbf{U}) + \lambda_1(\mathbf{V}) \le \lambda_k(\mathbf{U} + \mathbf{V}) \le \lambda_k(\mathbf{U}) + \lambda_n(\mathbf{V}) \tag{19}$$

Take $\mathbf{U}$ as $\mathbf{A} + \mathbf{A}^T$ and $\mathbf{V}$ as $c\mathbf{I}_N$. It is clear that if $c \ge \lambda_1(\mathbf{A} + \mathbf{A}^T)$ then $\mathbf{Q}$ will be positive semidefinite. The same also applies to $\mathbf{Q}_i$ and the constants c_i for the constraints.

The calculation for the eigenvalue for both the objective function and each of the constraints might seem time consuming. Nevertheless, we can simply use a predefined constant rather than calculating the eigenvalue for each optimization problem. In our simulation, simply choosing $c = c_i = 1$ is sufficient to ensure a valid MIQCQP formulation.

F. Extension to Multi-Cell Scenarios

We propose a scheduler based on the MIQCQP formulation in a downlink, single-cell setting in previous sections. The same formulation methodology can be applied to downlink cooperative multipoint (CoMP) scenarios with changes in the definition of variables and in the derivation of the normalized interference matrix $\mathbf{Z}$. Let us consider a downlink scheduler in a multi-cell network with C full frequency-reusing and synchronized cells. Suppose that N_k users are in cell $k, k = 1, \cdots, C$, and there is inter-cell interference (ICI) due to full frequency reuse among cells.

To distinguish the users in different cells, we use superscript to indicate the index of the cell and use the subscript to indicate the user in a specific cell. Define $\mathbf{h}_i^{k,l}$ as the normalized CIR from cell l to user i in cell k and define $\mathbf{g}_j^l$ as the transmitting waveform assigned to user j in cell l. Define $G_i^{k,l}$ as the path gain from cell l to the user i in cell k. Suppose all users in all cells use the same backoff factor D, then the downsampled received signal for user i in cell k can be expressed as (20), where the first term is the received signal, the second term the ISI, the third term the IUI, the fourth term is the ICI, and the last term is the receiving noise.

Let $\mathbf{Z}^{k,k}$ denote the N_k by N_k normalized interference matrix within cell k as defined in Sec.IV-B. Let $\mathbf{Z}^{k,l}$ be the N_k by N_l ICI matrix. $\mathbf{Z}_{i,j}^{k,l}$, the $(i,j)^{th}$ term of $\mathbf{Z}^{k,l}$, represents the ICI to the user i in cell k due to the transmitted signal to user j in cell l. $\mathbf{Z}_{i,j}^{k,l}$ is defined as

$$\mathbf{Z}_{i,j}^{k,l} = \sum_{t=0}^{\frac{2L-2}{D}} \frac{G_i^{k,l}}{G_i^{k,k}} \left|(\mathbf{h}_i^{k,l} * \mathbf{g}_j^l)[Dt]\right|^2,$$

where $G_i^{k,k}$ in the denominator is to cancel the same term later in the formulation. We can define the normalized interference

$$
\begin{aligned}
Y_i^k[s] &= \sum_{c=1}^{C}\sum_{u=1}^{N_c}\sum_{t}\sqrt{G_i^{k,c}p_u^c}X_u^c[t](\mathbf{h}_i^{k,c}*\mathbf{g}_u^c)[sD-tD]+n_i^k[s] \\
&=\sqrt{G_i^{k,k}p_i^k}X_i^k[s](\mathbf{h}_i^{k,k}*\mathbf{g}_i^k)[L-1]+\sqrt{G_i^{k,k}p_i^k}\sum_{t=0,t\neq\frac{L-1}{D}}^{\frac{2L-2}{D}}X_i^k[s-t](\mathbf{h}_i^{k,k}*\mathbf{g}_i^k)[Dt] \\
&\quad+\sum_{j\neq i}\sqrt{G_i^{k,k}p_j^k}\sum_{t=0}^{\frac{2L-2}{D}}X_j^k[s-t](\mathbf{h}_i^{k,k}*\mathbf{g}_j^k)[Dt]+\sum_{c=1,c\neq k}^{C}\sum_{j}\sqrt{G_i^{k,c}p_j^c}\sum_{t=0}^{\frac{2L-2}{D}}X_j^c[s-t](\mathbf{h}_i^{k,c}*\mathbf{g}_j^c)[Dt]+n_i^k[s],
\end{aligned}
\tag{20}
$$

$$
\begin{aligned}
&\underset{\hat{\mathbf{x}}}{\text{maximize}}\ \sum_k\sum_i w_i^k x_i^k\log_2\left(\frac{G_i^{k,k}p_i^k}{\left(G_i^{k,k}\tilde{\mathbf{Z}}\text{diag}(\hat{\mathbf{p}})\hat{\mathbf{x}}\right)[\sum_{c=1}^{k-1}N_c+i]+(\sigma_i^k)^2}+1\right) \\
&\text{subject to } x_i^k\in\{0,1\},\forall i,k,\quad \sum_i p_i^k x_i^k\le P_{max}^k,\forall k,\quad \frac{G_i^{k,k}p_i^k x_i^k}{\left(G_i^{k,k}\tilde{\mathbf{Z}}\text{diag}(\hat{\mathbf{p}})\hat{\mathbf{x}}\right)[\sum_{c=1}^{k-1}N_c+i]+(\sigma_i^k)^2}\ge\gamma_i^k x_i^k,\quad \forall i,k,
\end{aligned}
\tag{21}
$$

matrix $\tilde{\mathbf{Z}}$ in the multi-cell scenario as

$$
\tilde{\mathbf{Z}}=\begin{bmatrix}\mathbf{Z}^{1,1} & \mathbf{Z}^{1,2} & \cdots & \mathbf{Z}^{1,C}\\ \mathbf{Z}^{2,1} & \mathbf{Z}^{2,2} & \cdots & \mathbf{Z}^{2,C}\\ \vdots & \vdots & \ddots & \vdots\\ \mathbf{Z}^{C,1} & \mathbf{Z}^{C,2} & \cdots & \mathbf{Z}^{C,C}\end{bmatrix}.
$$

Let $\tilde{N}=\sum_{k=1}^{C}N_k$ be the total number of users in all cells, and we define the new decision variable vector of length $\tilde{N}$ as $\hat{\mathbf{x}}=[\mathbf{x}_1^T\ \ \mathbf{x}_2^T\ \ \cdots\ \ \mathbf{x}_C^T]^T$, and the new power vector of length $\tilde{N}$ as $\hat{\mathbf{p}}=[\mathbf{p}_1^T\ \ \mathbf{p}_2^T\ \ \cdots\ \ \mathbf{p}_C^T]^T$. The total interference $\mathcal{I}_i^k$ including ISI, IUI and ICI to user i in cell k is $\left(G_i^{k,k}\tilde{\mathbf{Z}}\text{diag}(\hat{\mathbf{p}})\hat{\mathbf{x}}\right)[\sum_{c=1}^{k-1}N_c+i]$, where the term in $(\cdot)$ is a vector of length $\tilde{N}$, and the operator $[\cdot]$ takes out the corresponding element in the vector.

The weighted sum rate maximization in (6) can be reformulated using the newly defined variables and interference matrix as (21), where user i in cell k has its own corresponding weight w_i^k, SINR requirements γ_i^k, and receiving noise $(\sigma_i^k)^2$. The same procedure follows to transform the optimization problem into the MIQCQP formulation. In the CoMP setting, it is assumed that the scheduler has the full knowledge of the path gain, channels, and waveforms of the system. If the full knowledge of the system is too expensive to obtain, some of the components can be approximated and the MIQCQP formulation still applies.

V. Impact of Imperfect Channel Information

In the previous Section, we assume that the CIR information provided by the physical layer to be perfect. However, the CIR information provided by the physical layer is subject to receiving noise. The mismatch between the true and the estimated channel causes worse energy focusing in the 5G system, which results in a lower SINR in communication. Moreover, the mismatch also degrades the scheduler performance by noisy physical layer parameter inputs.

To investigate the impact of imperfect channel information, we start from analyzing the channel estimation error of the physical layer. There is existing literature on the distribution of the channel estimation error for the massive MIMO system [19], but there is no existing analysis or models on the channel estimation error on the TR system. Therefore, we first analyze a Golay sequence based channel estimation scheme for TR system proposed in [14] and analyze its impact on the accuracy of scheduler parameter inputs.

A. Golay Sequence Based Channel Estimation

The Golay complementary sequence is first proposed in [20], which suggested a set of complementary sequence pairs $\mathbf{G}_a$ and $\mathbf{G}_b$ of the same length L_G. The correlation of $\mathbf{G}_a$ with itself, i.e. $\text{Corr}(\mathbf{G}_a,\mathbf{G}_a)$ has a prominent peak but noisy sidelobes. However, $\text{Corr}(\mathbf{G}_a,\mathbf{G}_a)+\text{Corr}(\mathbf{G}_b,\mathbf{G}_b)$ produces a single maximum peak with no sidelobes. This prominent peak is useful in channel estimation because a clean copy of channel estimation can be obtained at the peak without the interference from the sidelobes.

Generation of $\mathbf{G}_a$ and $\mathbf{G}_b$ is based on two different sequences D_n and W_n of length n, and the length of the generated Golay sequence is $L_G=2^n$. Fig. 3 shows an example of $\mathbf{G}_a$ and $\mathbf{G}_b$ pair using randomly generated D_n and W_n with $L_G=256$, and $\text{Corr}(\mathbf{G}_a,\mathbf{G}_a)+\text{Corr}(\mathbf{G}_b,\mathbf{G}_b)$ shows a clear peak with no sidelobes. Please note that the amplitude of the peak is $2L_G$ and the length of the zero at the two sides of the peak is L_G-1.

B. Channel Estimation via Golay Sequence

A channel estimation scheme using a $8L_G$ by 1 probing sequence ϕ is proposed in [14], which is composed of the corresponding pair of Golay sequences $\mathbf{G}_a,\mathbf{G}_b$ as

$$
\phi=[\mathbf{G}_a^T\ \ \mathbf{G}_b^T\ \ -\mathbf{G}_a^T\ \ \mathbf{G}_b^T\ \ \mathbf{G}_a^T\ \ -\mathbf{G}_b^T\ \ \mathbf{G}_a^T\ \ \mathbf{G}_b^T]^T. \tag{22}
$$

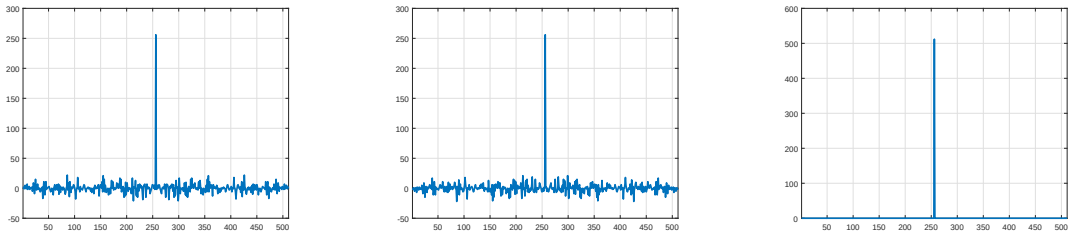

(a) $\mathbf{G}_a$. (b) $\mathbf{G}_b$. (c) Corr($\mathbf{G}_a, \mathbf{G}_a$) + Corr($\mathbf{G}_a, \mathbf{G}_a$).

Fig. 3: An example of Golay sequence.

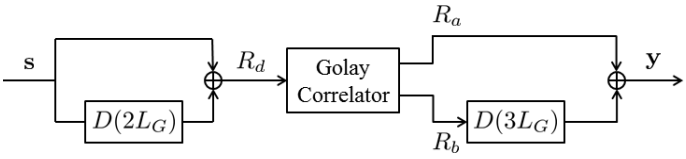

Fig. 4: Diagram for Golay based channel estimation.

Fig. 4 shows the block diagram of the channel estimation. The transmitter transmits the channel estimation sequence ϕ and the receiver receives the $L+8L_G-1$ by 1 signal $\mathbf{s} = \phi * \mathbf{h} + \mathbf{n}$, where L is the length of $\mathbf{h}$. We assume $\mathbf{n}$ is AWGN with zero mean and variance σ^2.

The received signal $\mathbf{s}$ is divided into two branches. One branch goes through a delay of $2L_G$ and is summed with the other branch as $\mathbf{R}_d$.

$$\mathbf{R}_d = \left(\begin{bmatrix} \mathbf{I}_L \\ \mathbf{0}_{2L_G,L} \end{bmatrix} + \begin{bmatrix} \mathbf{0}_{2L_G,L} \\ \mathbf{I}_L \end{bmatrix} \right) \mathbf{s}. \tag{23}$$

We calculate the correlation of $\mathbf{R}_d$ with $\mathbf{G}_a$ and $\mathbf{G}_b$ using the Golay correlator block, which produces two branches $\mathbf{R}_a$ and $\mathbf{R}_b$, respectively. Define C_a and C_b as the $L+3L_G-1$ by $L+2L_G$ convolution matrix constructed by the time-reversed version of $\mathbf{G}_a$ and $\mathbf{G}_b$, and the outputs of the Golay correlator can be expressed as $\mathbf{R}_a = C_a\mathbf{R}_d$ and $\mathbf{R}_b = C_b\mathbf{R}_d$. $\mathbf{R}_b$ is delayed by $3L_G$ to summed with $\mathbf{R}_a$ in order to produce the final channel estimation result. Therefore, the whole estimation block can be expressed as

$$\begin{aligned} \mathbf{y} &= \begin{bmatrix} \mathbf{I}_{L+3L_G-1} \\ \mathbf{0}_{2L_G,L+3L_G-1} \end{bmatrix} C_a\mathbf{R}_d + \begin{bmatrix} \mathbf{0}_{2L_G,L+3L_G-1} \\ \mathbf{I}_{L+2L_G-1} \end{bmatrix} C_b\mathbf{R}_d \\ &= T(\phi * \mathbf{h} + \mathbf{n}) = \begin{bmatrix} T_1 \\ \Phi \\ T_2 \end{bmatrix} (\phi * \mathbf{h} + \mathbf{n}). \end{aligned} \tag{24}$$

The matrix T is the total transfer function from the estimation block input $\mathbf{s}$ to the block output, and it is separated into three parts T_1, Φ, and T_2 by the rows. T_1 and T_2 represent the noisy part of the channel estimation scheme which is the sidelobes of the correlation of G_a and G_b, and these two parts are of no interest in channel estimation. Φ is the $(7L_G)^{th}$ to the $(8L_G)^{th}$ rows that correspond to the clean peak of the correlation of the Golay sequences without sidelobes, as shown in Fig. 3(c). Φ is a matrix that is determined by the Golay sequence pair, and each row of Φ has exact $4L_G$ none zeros entries with amplitude 1.

The channel estimation $\hat{\mathbf{h}}$ of length L_G+1 can therefore be represented as

$$\hat{\mathbf{h}} = \Phi(\phi * \mathbf{h} + \mathbf{n}) = 4L_G\mathbf{h}' + \Phi\mathbf{n} = 4L_G\mathbf{h}' + \mathbf{n}_e, \tag{25}$$

where $\mathbf{h}'$ is of length L_G+1 which is formed by zero-padding $\mathbf{h}$ to match the matrix dimension, and $\mathbf{n}_e$ is the channel estimation error due to the received noise $\mathbf{n}$ at the receiver.

C. Channel Estimation Error Analysis

We investigate the mean and variance of $\mathbf{n}_e$ to show the effect of $\mathbf{n}$ and L_G on the quality of channel estimation. By the assumption that $\mathbf{n}$ is AWGN with zero mean and variance σ^2, the mean of estimation error $\mathbf{n}_e$ is also zero. The covariance of the channel estimation error $\mathbf{n}_e$ is $\Phi\text{Cov}(\mathbf{n})\Phi^H$. It is assumed that $\mathbf{n}$ is i.i.d. AWGN with variance σ^2, and therefore the covariance of $\mathbf{n}_e$ is $\sigma^2\Phi\Phi^H$.

To give an example of the correlation of $\mathbf{n}_e$, we randomly generate a Golay sequence pair with $L_G = 256$. Fig. 5 is the correlation of $\mathbf{n}_e$ with $\mathbf{n}$ to be i.i.d. Gaussian with unit σ^2, namely $\Phi\Phi^H$. The prominent diagonal components have value $4L_G$ and each element of the diagonal is the noise variance σ_e^2 of $\mathbf{n}_e$. The off-diagonal components have extremely low value, which shows that different components of $\mathbf{n}_e$ are almost uncorrelated. Therefore, the channel estimation errors $\mathbf{n}_e$ on each tap of the estimated channel $\mathbf{h}'$ are nearly uncorrelated, which is nearly independent due to the assumption that $\mathbf{n}$ is i.i.d. AWGN.

D. SNR Enhancement of Golay Sequence Based Channel Estimation

The Golay sequence based channel estimation scheme increases the SNR of the channel estimation. Suppose that the SNR at the receiver is P/σ^2 where P and σ^2 are the power of the received signal $\mathbf{s}$ and the noise $\mathbf{n}$, respectively. The channel estimation output has a peak with amplitude $4L_G$, by which the power of the channel estimation is $16L_G^2P$. Each row of Φ consists of exactly $4L_G$ none zero elements with amplitude 1, therefore σ_e^2 is $4L_G\sigma^2$. As a result, the SNR at the channel estimation output is boosted for $4L_G$ times.

The channel estimate using the proposed Golay channel estimation scheme is contaminated with noise which has zero mean and variance $4L_G\sigma^2$. Therefore, the length of the Golay sequence affects the SNR boost at the estimation output, and the TR system can adapt the Golay sequence length L_G

$$\mathbb{E}\left[\hat{\mathbf{Z}}_{i,j}\right] = \mathbb{E}\left[\sum_{l=0}^{\frac{2L-2}{D}} \left|(\hat{\mathbf{h}}_i * \mathbf{g}_j)[Dl]\right|^2\right] = \mathbb{E}\left[\sum_{l=0}^{\frac{2L-2}{D}} \left|\left((\mathbf{h}_i + \mathbf{n}_e) * \mathbf{g}_j\right)[Dl]\right|^2\right]$$

$$= \begin{cases} \mathbf{Z}_{i,j} + \dfrac{\sigma^2}{4L_G}\left(\dfrac{L-1}{D} - 1\right) + \dfrac{\sigma^2}{4L_G}\displaystyle\sum_{l=0}^{\frac{L-1}{D}} \left|\mathbf{g}_j[Dl]\right|^2 & , \text{if } i = j \\ \mathbf{Z}_{i,j} + \dfrac{\sigma^2}{4L_G}\left(\dfrac{L-1}{D}\right) + \dfrac{\sigma^2}{4L_G}\displaystyle\sum_{l=0}^{\frac{L-1}{D}} \left|\mathbf{g}_j[Dl]\right|^2 & , \text{if } i \neq j \end{cases} < \begin{cases} \mathbf{Z}_{i,j} + \dfrac{\sigma^2}{4L_G}\left(\dfrac{L-1}{D}\right) & , \text{if } i = j \\ \mathbf{Z}_{i,j} + \dfrac{\sigma^2}{4L_G}\left(\dfrac{L-1}{D} + 1\right) & , \text{if } i \neq j \end{cases} \quad (26)$$

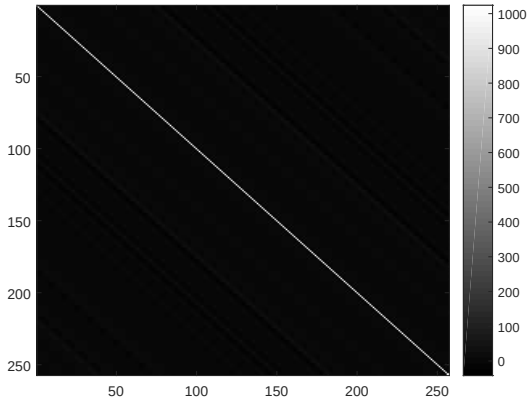

Fig. 5: An example of $\Phi\Phi^H$.

based on the system requirement on channel estimation. More importantly, $\mathbf{n}_e$ on each tap of the channel estimation are nearly independent, which is the result of the structure of the transfer function Φ of the Golay channel estimation scheme.

The channel estimation error for the massive MIMO system is investigated in [19]. The channel estimation errors on the links from the base station to a user are i.i.d. complex Gaussian with zero mean and same variance which is determined by the shadowing effect of the user. The channel estimation error of the TR system and the massive MIMO system share the similarity in that the estimation errors of the channel are i.i.d variables with zero mean and the same variance. This similarity in channel estimation error therefore extends the discussion and simulation results on the scheduler performance degradation to massive MIMO counterparts.

E. Effect on the Scheduler Parameter

The proposed scheduler algorithm generates the transmission profile for the users based on the estimated channel and the assigned power from the physical layer. Inaccurate channel estimation deteriorates the efficiency of the scheduling in the MAC layer, and it is desirable to investigate how the channel estimation error affects the input parameter of the proposed scheduler.

Based on the previous investigation of the channel estimation error, we model the estimated channel $\hat{\mathbf{h}}$ as

$$\hat{\mathbf{h}} = \mathbf{h} + \mathbf{n}_e,$$

where we assume that $\mathbf{n}_e$ is i.i.d. complex Gaussian noise with zero mean and variance σ_e^2. According to the optimization formulation of the scheduler in (6), channel estimation error $\mathbf{n}_e$ affects the scheduler performance by affecting the calculation of the normalized interference matrix $\mathbf{Z}$. Define $\hat{\mathbf{Z}}$ as the normalized interference matrix obtained using the channel estimation $\hat{\mathbf{h}}$, and we calculate the expectation of $\hat{\mathbf{Z}}$ to show the impact of channel estimation error on the normalized interference matrix $\mathbf{Z}$. $\mathbf{Z}$ is shown in (26), where the last inequality results from the normalized waveform $\mathbf{g}_j$ and serves as an upper bound for $\mathbb{E}\left[\hat{\mathbf{Z}}\right]$.

The formula suggests that the error in the normalized interference matrix $\Delta\mathbf{Z} = \mathbb{E}\left[\hat{\mathbf{Z}}_{i,j}\right] - \mathbf{Z}_{i,j}$ relates to three factors, the backoff factor D, the channel length L, and the length of the Golay sequence L_G. A larger backoff factor not only reduces the IUI and ISI but also reduces the impact of the channel estimation error on the normalized interference matrix. The longer the channel length, the larger the IUI and ISI, thus the bigger $\Delta\mathbf{Z}$. The last factor is the Golay sequence length L_G, which affects the additive noise power at the channel estimation. The dependence of n_e on L_G gives the system the flexibility to adapt the length of Golay sequence to the users' SNR conditions.

VI. Simulation Results

In this section, we evaluate the performance of the proposed scheduler algorithm from several aspects. First, we compare the time complexity of the proposed scheduler algorithm with that using enumeration. We also evaluate the scheduler performance under different physical layer structures. Then we investigate the impact of channel estimation error. We use the following model and system parameters. We generate $\mathbf{h}$ of the TR system based on the channel model proposed in [4], where $h_i[k] = \sum_{l=0}^{L-1} h_{i,l}\delta[k-l]$. $h_i[k]$ is the k-th tap of the CIR with length L, and δ is the Dirac delta function. We assume that $h_i[k]$ are independent circular symmetric complex Gaussian (CSCG) random variables with zero mean and variance as $E[|h_i[k]|^2] = e^{-\frac{kT_S}{\sigma_T}}$, $0 \leq k \leq L-1$. T_S is the sampling period of the system, which is 8 nanoseconds for the 125 MHz system. σ_T is the root mean square delay spread of the channel, which is about 30 to 50 nanoseconds in an indoor environment. We select L to be 30 since most of the channel energy is concentrated in this part. The waveform $\mathbf{g}$ is the time reversed and conjugated version of $\mathbf{h}$. For TR system, users

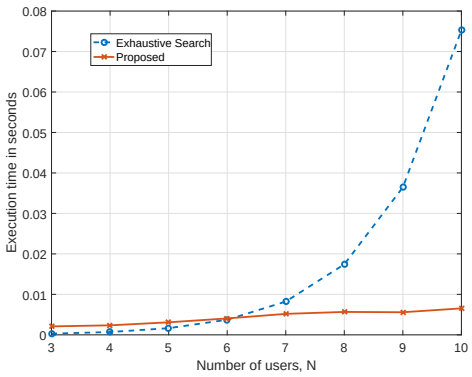

Fig. 6: Run time comparison for different number of users.

are distributed randomly within a 20 meter by 20 meter area with the transmitter located at the center to simulate an indoor environment. For massive MIMO system, users are distributed randomly within a 300 meter by 300 meter area to simulate an outdoor environment. The transmitter is located at the center of the area in both cases. The path loss exponent is 3.5. The rate requirements for the users R_i are generated uniformly from the range of 1 Mbps to 2 Mbps. The weight vector $\mathbf{w}$ is generated uniformly from 0 to 1. The power vector is generated from a uniform distribution from 0.1 to 0.3 for each user and P_{max} is set to 1. The SNR is 0 dB for each of the users unless mentioned otherwise. The system bandwidth of the TR system is 125 MHz in the simulation. The simulation is repeated for 2000 channel realizations for each of the settings. Lastly, we select the Gurobi solver to solve the MIQCQP problem [21].

A. Time Complexity

Time complexity is an important performance indication for a scheduler that performs in real time with a strict deadline. Moreover, the importance grows with the foreseeable sharp increase in the number of users in the system. Fig. 6 shows the comparison of the running time with number of users N ranging from 3 to 10 and $D = 4$. The proposed scheduler consumes more time than that of exhaustive search when the number of users is small due to the model setup and shows an empirical $O(N)$ complexity. The result shows $O(2^N)$ complexity for exhaustive search and the execution time outpaces the proposed scheduler. The $O(N)$ complexity makes the proposed scheduler suitable for application with a strict deadline.

B. Scheduling Performance Comparison

To evaluate the performance of the proposed scheduler, we compare the weighted sum rate of the proposed scheduler R_S with the weighted sum rate obtained by exhaustive search R_{opt} by calculating the average of the ratio $\rho = R_S/R_{opt}$. We chose the backoff factor $D = [4, 8, 12, 24, 30]$ and number of users $N = [3, 5, 7, 9]$. Fig. 7(a) shows the ρ with different N and D. For a small D, the deviation from optimality with large N comes from the errors at the linearization of the logarithm term around 1, because the actual sum is far from 1. However, when D increases, the entries of $\mathbf{Z}$ becomes smaller and the error due to expansion at 1 gets smaller. For larger N, which is the targeted use case for the next generation system, ρ increases rapidly to above 0.9 in all cases where D is larger than 8.

To evaluate the performance of the proposed scheduler under different SNR conditions, we perform simulations where all users have the same SNR selected from $[-5, 0, 5, 10]$ dB. We simulate with different backoff factors $D = [4, 8, 12, 24, 30]$ and $N = 9$, and the result is presented in Fig. 7(b). In the low SNR region, the approximation in (8) is not as accurate and there is a gap between the performance of the proposed scheduler and that of exhaustive search. However, ρ increases over 0.9 when D is larger than 8 in most SNR cases.

The proposed scheduler separates the physical layer implementation, and the separation makes the scheduler suitable for different waveform design and power allocation algorithms. Fig. 8(a) shows ρ with a downlink system using the waveform design and power allocation proposed in [16]. The original uplink max-min SINR algorithm in [16] is modified using the uplink-downlink duality for downlink purpose. The figure shows a similar ρ as in Fig. 7(a), which shows that the proposed scheduler algorithm is versatile for different physical layer implementation.

We also evaluate the scheduler performance on the massive MIMO system. We assume flat fading channels, i.e. one tap channel, on each link of the massive MIMO system. Each link is modeled as a complex Gaussian random variable with zero mean and unit power as $CN(0, 1)$. The beamforming vector $\mathbf{g}_i$ is selected as the maximum ratio combining (MRC) scheme, where $\mathbf{g}_i$ is simply the complex conjugate of the channel link $\mathbf{h}_i^*$. We set the number of users $N = [3, 7, 10, 13]$ and the number of antennas $M = [10, 20, 30, 40]$ and simulate 2000 channel realizations. Fig. 8(b) shows ρ of the proposed scheduler and it is obvious that ρ approaches to 1 in all cases we simulated.

To evaluate the performance of the scheduler with a large number of users, we evaluate the scheduler performance with the number of users $N = [15, 20, 25, 30]$ and $D = [16, 20, 25]$. We compare the average weighted sum rate of the scheduler output with a first-come-first-serve system that tries to accommodate as much as users as possible given the users' requirements are satisfied. We simulate 4000 channel realizations for each set of N and D and Fig. 9 shows the results of the two schedulers. The result shows that the proposed scheduler outperforms the first-come-first-serve system in every setting by a large margin, showing the effectiveness of the scheduler with a large N. With a fixed D, the weighted sum rate increases with N and saturate when N is large. The SINR requirements of the users limit the achievable regions of the system and results in the weighted sum rate saturation at larger N. With a fixed N, the system weighted sum rate decrease with larger D because of less frequent transmission.

To evaluate the scheduler performance with existing schedulers, we compare the performance with the massive MIMO scheduler proposed in [22]. The authors proposed a pair-wise semi-orthogonal user selection (pair-wise SUS) scheduler that selects transmitting users with mutual channel correlations lower than a cut-off value β_{min}. We select β_{min} to be 0.45 which shows the best performance across a different number

This article has been accepted for publication in a future issue of this journal, but has not been fully edited. Content may change prior to final publication. Citation information: DOI 10.1109/TWC.2017.2690432, IEEE Transactions on Wireless Communications

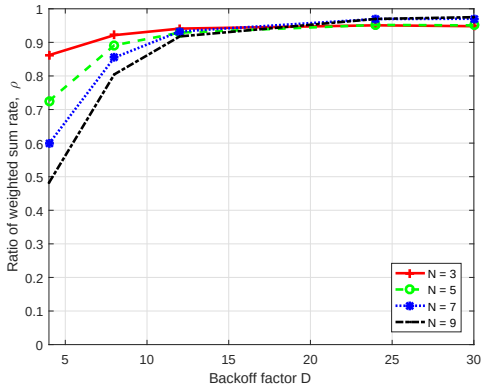

(a) Performance with different number of users.

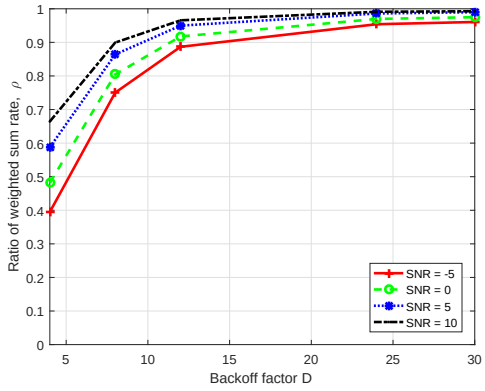

(b) Performance under different SNR conditions.

Fig. 7: Performance of the proposed scheduler compared with exhaustive search result.

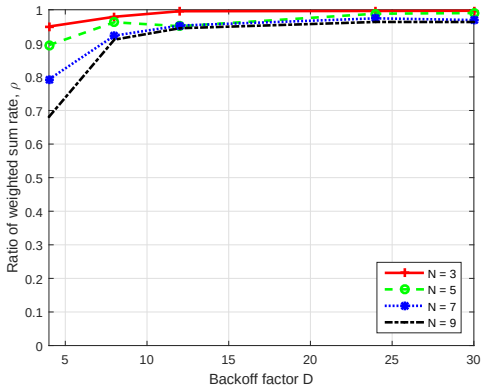

(a) Performance using waveform design algorithm proposed in [16].

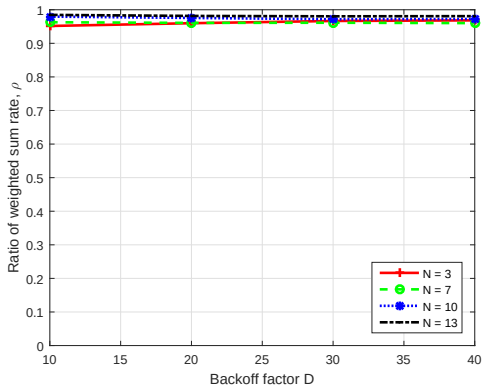

(b) Performance on massive MIMO system.

Fig. 8: Performance of the proposed scheduler with different physical layer implementations.

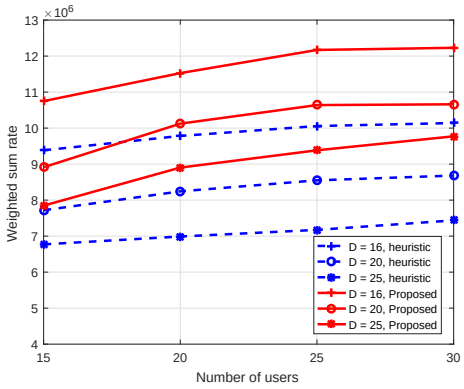

Fig. 9: Performance of proposed scheduler compared with a first-come-first-serve system.

of antennas at the transmitter in [22]. We impose the rate constraints on the users selected by pair-wise SUS scheduler and remove users one by one until all users' rate constraints are satisfied. We simulate 150 antennas at the transmitter, and 30 to 100 users in the system. We assume that each user has the same weight and simulate 2000 channel realizations. The performance metric is measured by the complexity and the average ratio $\rho_{SUS} = R_S/R_{SUS}$ of the system sum rates between the proposed scheduler (R_S) and the pair-wise SUS scheduler (R_{SUS}).

Fig. 10(a) shows the mean execution time of the pair-wise SUS scheduler and the proposed scheduler. Simulation result shows that the proposed scheduler has $O(N)$ complexity, while pair-wise SUS scheduler has $O(N^2)$ complexity, where N is the number of users. The $O(N^2)$ complexity of the pair-wise SUS scheduler is the result of the need to search through all pairs of users' channels to find the high correlated pairs and to remove one of them in the selected user set.

Fig. 10(b) shows the ρ_{SUS} of the pair-wise SUS scheduler and the proposed scheduler. The simulation shows that the proposed scheduler outperforms the pair-wise SUS scheduler in all cases, and ρ increases with the increase of users. The pair-wise SUS scheduler removes users with high channel correlation one-by-one, and therefore the selection process of the scheduler may reach a local optimum. On the other hand, the proposed scheduler selects users together, and therefore the global optimal value of the MIQCQP formulation can be

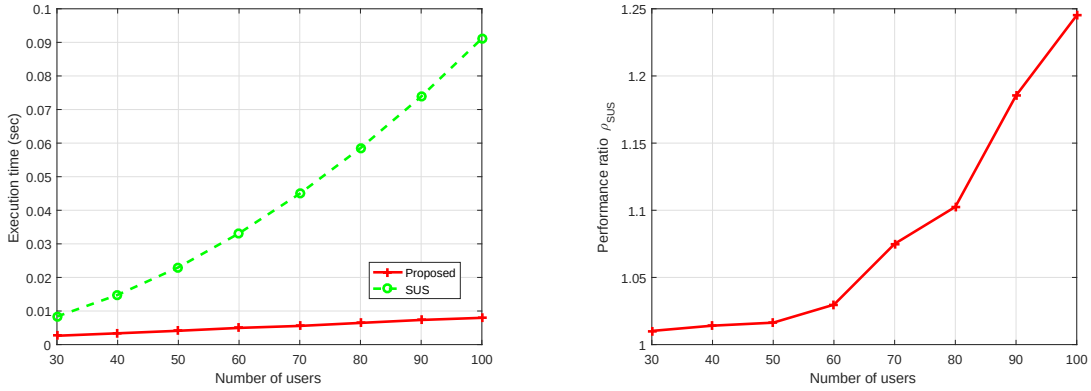

(a) Time complexity comparison.

(b) Performance ratio ρ_{SUS}.

Fig. 10: Performance comparison between the proposed scheduler and the pair-wise SUS scheduler.

L_G	16	32	64	128	256
$r_{i,j}$	0.187	0.145	0.0118	0.093	0.081

TABLE I: Maximum absolute value of the off-diagonal components of the estimated channel estimation error correlation with different L_G.

reached.

C. Channel Estimation Error

To investigate the distribution of the channel estimation error, we simulate the estimation error of the Golay channel estimation block output as follows. We generate i.i.d. AWGN $\mathbf{n}$ with zero mean and unit variable at the receiver input. We randomly generate 100 pairs of Golay sequence with length $L_G = [16, 32, 64, 128, 256]$. For each pair of the Golay sequences, we generate 10000 realizations of $\mathbf{n}$ and estimate the correlation coefficient of the channel estimation error at the output, i.e. the correlation of $\mathbf{n}_e$.

Table. I shows the maximum absolute value of the off-diagonal element of the estimated correlation $r_{i,j}, i \neq j$ of $\mathbf{n}_e$ over all the 100 random realizations of the Golay sequence. With the increase of L_G, $\max(r_{i,j}), i \neq j$ decreases to less than 0.1 which indicates that the channel estimation error has low correlation value. This justifies our previous assumption that the channel estimation error on each tap of channel estimation at the output of the Golay based estimation block can be modeled as independent. Also, the Golay sequence in the simulation is generated via random realizations of D_n and W_n, and exhaustive search on D_n and W_n can further reduce $r_{i,j}$ if desirable.

We evaluate the effect of channel estimation error on the stability of the scheduler performance as the following. We assume the SNR at the receiver is 0dB and calculate the corresponding channel estimation noise power with different Golay sequence length L_G. Then we calculate $\mathbf{Z}$ with the estimated channel $\hat{\mathbf{h}}_i$ and $\mathbf{g}_j$ being the time-reversed and conjugated CIR. Then we calculate the ratio ρ_E between the scheduler output with channel estimation error R_E and the scheduler output with perfect channel information R_S. We perform 2000 realizations and calculate the mean of ρ_E in all cases.

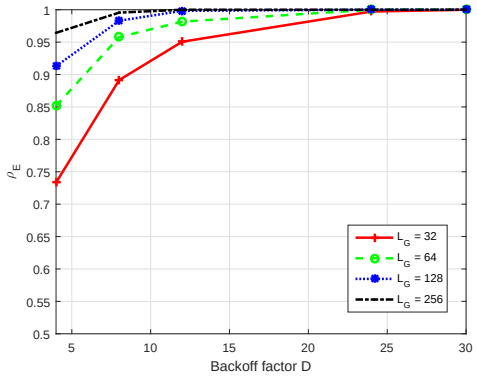

Fig. 11: Performance ratio ρ_E between perfect channel R_S and channel estimation error R_E.

Fig. 11 shows the ratio ρ_E with $N = 9$, where the y-axis runs from 0.5 to 1. A small L_G does affect the scheduler performance, but the performance reduction reduces with a larger L_G. Moreover, for the range where $D > 8$ which is a preferable operating point for $N = 9$, the reduction in performance is marginal. The result shows that the proposed scheduler is robust against channel estimation error and the system can adjust the Golay sequence length according to the SNR of the received signal.

VII. Conclusion

In this paper, we propose a novel scheduler for the 5G downlink system. The scheduler objective of maximizing system weighted throughput and the SINR constraints of the users are transformed into an MIQCQP problem. The proposed schduler has a linear complexity compared to the exponential complexity of exhaustive search with slight performance reduction. Secondly, we investigate the impact of imperfect channel information and analyze a channel estimation scheme of TR system using Golay sequence pairs. The Golay sequence

based channel estimation error has a similar distribution as the channel estimation error of the MIMO system. The proposed scheduler is shown to be robust against channel estimation error and is versatile for different physical layer structures. The robustness, versatility, and the low time complexity make the proposed scheduler suitable for deployment in systems with a massive number of users and strict scheduling deadlines.

REFERENCES

[1] Y. Chen, F. Han, Y.H. Yang, H. Ma, Yi Han, C. Jiang, H.Q. Lai, D. Claffey., Z. Safar, and K.J.R. Liu, "Time-reversal wireless paradigm for green internet of things: An overview," *IEEE Internet Things J.*, vol. 1, no. 1, pp. 81–98, Feb 2014.

[2] Y. Chen, B. Wang, Y. Han, H. Q. Lai, Z. Safar, and K. J. R. Liu, "Why time reversal for future 5G wireless?," *IEEE Signal Process. Mag.*, vol. 33, no. 2, pp. 17–26, Mar 2016.

[3] Z.H. Wu, Y. Han, Y. Chen, and K.J.R Liu, "A time-reversal paradigm for indoor positioning system," *IEEE Veh. Technol. Mag.*, vol. 64, no. 4, pp. 1331–1339, Apr 2015.

[4] F. Han, Y.H. Yang, B. Wang, Y. Wu, and K.J.R. Liu, "Time-reversal division multiple access over multi-path channels," *IEEE Trans. Commun.*, vol. 60, no. 7, pp. 1953–1965, Jul 2012.

[5] E. Larsson, O. Edfors, F. Tufvesson, and T. Marzetta, "Massive MIMO for next generation wireless systems," *IEEE Commun. Mag.*, vol. 52, no. 2, pp. 186–195, Feb 2014.

[6] A. Pokhariyal, K.I. Pedersen, G. Monghal, I.Z. Kovacs, C. Rosa, T.E. Kolding, and P.E. Mogensen, "HARQ aware frequency domain packet scheduler with different degrees of fairness for the UTRAN long term evolution," in *Vehicular Technology Conf.*, Apr 2007, pp. 2761–2765.

[7] R. Kwan, C. Leung, and J. Zhang, "Proportional fair multiuser scheduling in LTE," *IEEE Signal Process. Lett.*, vol. 16, no. 6, pp. 461–464, Jun 2009.

[8] C. Wengerter, J. Ohlhorst, and A.G.E. von Elbwart, "Fairness and throughput analysis for generalized proportional fair frequency scheduling in OFDMA," in *Vehicular Technology Conf.*, May 2005, vol. 3, pp. 1903–1907.

[9] J. Huang, V.G. Subramanian, R. Agrawal, and R.A. Berry, "Downlink scheduling and resource allocation for OFDM systems," *IEEE Trans. Wireless Commun.*, vol. 8, no. 1, pp. 288–296, Jan 2009.

[10] H. Yin, D. Gesbert, and L. Cottatellucci, "Dealing with interference in distributed large-scale MIMO systems: A statistical approach," *IEEE J. Sel. Topics Signal Process.*, vol. 8, no. 5, pp. 942–953, Oct 2014.

[11] D.W.K. Ng and R. Schober, "Energy-efficient resource allocation in OFDMA systems with large numbers of base station antennas," in *Int. Conf. Communications*, Jun 2012, pp. 5916–5920.

[12] Y. Huang, C. W. Tan, and B. D. Rao, "Joint beamforming and power control in coordinated multicell: Max-min duality, effective network and large system transition," *IEEE Trans. Wireless Commun.*, vol. 12, no. 6, pp. 2730–2742, Jun 2013.

[13] L.A. Wolsey, *Integer Programming*, Wiley Series in Discrete Mathematics and Optimization. Wiley, 1998.

[14] H. Ma, Y. Han, Y. Chen, Z. Safar, F. Han, and K.J.R. Liu, "Handshaking protocol for time-reversal system," US Patent, 9313020, April 12, 2016.

[15] Yu-Han Yang, Beibei Wang, W.S. Lin, and K.J.R Liu, "Near-optimal waveform design for sum rate optimization in time-reversal multiuser downlink systems," *IEEE Trans. Wireless Commun.*, vol. 12, no. 1, pp. 346–357, Jan 2013.

[16] Q. Xu, Y. Chen, and K. Liu, "Combating strong-weak focusing effect in time-reversal uplinks," *IEEE Trans. Wireless Commun.*, vol. 15, no. 1, pp. 568 – 580, Jan 2015.

[17] H.Q. Ngo, E.G. Larsson, and T.L. Marzetta, "Massive MU-MIMO downlink TDD systems with linear precoding and downlink pilots," in *Annu. Allerton Conf. on Communication, Control, and Computing*, Oct 2013, pp. 293–298.

[18] R.A. Horn and C.R. Johnson, Eds., *Matrix Analysis*, Cambridge University Press, New York, NY, USA, 1986.

[19] H. Q. Ngo, E. G. Larsson, and T. L. Marzetta, "Energy and spectral efficiency of very large multiuser MIMO systems," *IEEE Trans. Commun.*, vol. 61, no. 4, pp. 1436–1449, Apr 2013.

[20] M. Golay, "Complementary series," *IRE Transactions on Information Theory*, vol. 7, no. 2, pp. 82–87, Apr 1961.

[21] Inc. Gurobi Optimization, "Gurobi optimizer reference manual," 2015.

[22] S. Dierks and N. Juenger, "Scheduling for massive MIMO with few excess antennas," in *20th Int. ITG Workshop Smart Antennas*, March 2016, pp. 1–5.

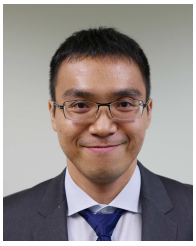

Zhung-Han Wu (S14) received the B.S. degree and the M.S. degree in electrical engineering from National Taiwan University, Taipei, Taiwan, in 2008 and 2010, respectively. He received the Ph.D. degree in electrical engineering from the University of Maryland, College Park in 2016. He is currently with Origin Wireless Inc., where he develops cloud-based smart radio algorithms and solutions for a wide variety of applications, including indoor positioning, tracking, and security monitoring. Dr. Wu received the A. James Clark School of Engineering Distinguished Graduate Fellowship in 2011 and was recognized as a distinguished teaching assistant of the University of Maryland in 2013.

BeiBei Wang (SM15) received the B.S. degree in electrical engineering (with the highest honor) from the University of Science and Technology of China, Hefei, in 2004, and the Ph.D. degree in electrical engineering from the University of Maryland, College Park in 2009. She was with the University of Maryland as a research associate in 2009-2010, and with Qualcomm Research and Development in 2010-2014. Since 2015, she has been with Origin Wireless Inc. as a principal technologist. Her research interests include wireless communications and signal processing. Dr. Wang received the Graduate School Fellowship, the Future Faculty Fellowship, and the Deans Doctoral Research Award from the University of Maryland, and the Overview Paper Award from IEEE Signal Processing Society in 2015. She is a co-author of Cognitive Radio Networking and Security: A Game-Theoretic View (Cambridge University Press, 2010).

Chunxiao Jiang (S'09-M'13-SM'15) received the B.S. degree in information engineering from Beihang University, Beijing in 2008 and the Ph.D. degree in electronic engineering from Tsinghua University, Beijing in 2013, both with the highest honors. Currently, he is an assistant research fellow in Tsinghua Space Center, Tsinghua University. His research interests include application of game theory, optimization, and statistical theories to communication, networking, signal processing, and resource allocation problems, in particular space information networks, heterogeneous networks, social networks, and big data privacy. He was the recipient of the Best Paper Award from IEEE GLOBECOM in 2013, the Best Student Paper Award from IEEE GlobalSIP in 2015, the Distinguished Dissertation Award from CAAI (Chinese Association for Artificial Intelligence) in 2014 and the Tsinghua Outstanding Postdoc Fellow Award (only ten winners each year) in 2015. He is a senior member of IEEE.

K.J. Ray Liu (F03) was named a Distinguished Scholar-Teacher of University of Maryland, College Park, in 2007, where he is Christine Kim Eminent Professor of Information Technology. He leads the Maryland Signals and Information Group conducting research encompassing broad areas of information and communications technology with recent focus on smart radios for smart life.

Dr. Liu was a recipient of the 2016 IEEE Leon K. Kirchmayer Technical Field Award on graduate teaching and mentoring, IEEE Signal Processing Society 2014 Society Award, and IEEE Signal Processing Society 2009 Technical Achievement Award. Recognized by Thomson Reuters as a Highly Cited Researcher, he is a Fellow of IEEE and AAAS.

Dr. Liu is a member of IEEE Board of Director. He was President of IEEE Signal Processing Society, where he has served as Vice President Publications and Board of Governor. He has also served as the Editor-in-Chief of IEEE Signal Processing Magazine.

He also received teaching and research recognitions from University of Maryland including university-level Invention of the Year Award; and college-level Poole and Kent Senior Faculty Teaching Award, Outstanding Faculty Research Award, and Outstanding Faculty Service Award, all from A. James Clark School of Engineering.